Transition between metamaterial and photonic-crystal behavior in arrays of dielectric rods

F. Dominec,[1,2] **C. Kadlec,**[1] **H. Němec,**[1] **P. Kužel,**[1] **and F. Kadlec**[1,*]

[1]*Institute of Physics, Academy of Sciences of the Czech Republic, Na Slovance 2, 18221, Prague 8, Czech Republic*

[2]*Department of Physical Electronics, Faculty of Nuclear Sciences and Physical Engineering, Czech Technical University, 11519, Prague 1, Czech Republic*

[*]*kadlecf@fzu.cz*

Abstract: Using finite-difference time-domain simulations, we study the interactions of electromagnetic radiation with a square array of dielectric rods parallel to the electric vector. We observe the electric and magnetic Mie resonances which induce intervals of negative effective permittivity and permeability and which contribute to the formation of the photonic band gaps. Owing to the interplay of these phenomena, a narrow spectral range with a negative refractive index can occur. However, this requires the filling fraction of the dielectric to fall into a well defined interval of values and its permittivity to exceed a minimum of about 50. We discuss these phenomena from the perspective of both photonic crystal and metamaterial concepts.

OCIS codes: (160.3918) Metamaterials; (160.5298) Photonic crystals.

References and links

1. E. Yablonovitch, "Inhibited spontaneous emission in solid-state physics and electronics," Phys. Rev. Lett. **58**, 2059–2062 (1987).
2. E. Yablonovitch, T. J. Gmitter, R. D. Meade, A. M. Rappe, K. D. Brommer, and J. D. Joannopoulos, "Donor and acceptor modes in photonic band structure," Phys. Rev. Lett. **67**, 3380–3383 (1991).
3. J. B. Pendry, A. J. Holden, W. J. Stewart, and I. Youngs, "Extremely low frequency plasmons in metallic mesostructures," Phys. Rev. Lett. **76**, 4773–4776 (1996).
4. J. Pendry, A. Holden, D. Robbins, and W. Stewart, "Magnetism from conductors and enhanced nonlinear phenomena," IEEE Trans. Microw. Theo. and Techn. **47**, 2075–2084 (1999).
5. J. B. Pendry, "Negative refraction makes a perfect lens," Phys. Rev. Lett. **85**, 3966–3969 (2000).
6. D. R. Smith, W. J. Padilla, D. C. Vier, S. C. Nemat-Nasser, and S. Schultz, "Composite medium with simultaneously negative permeability and permittivity," Phys. Rev. Lett. **84**, 4184–4187 (2000).
7. V. M. Shalaev, "Optical negative-index metamaterials," Nat. Photon. **1**, 41–48 (2007).
8. H.-T. Chen, W. J. Padilla, J. M. O. Zide, A. C. Gossard, A. J. Taylor, and R. D. Averitt, "Active terahertz metamaterial devices," Nature **444**, 597 (2006).
9. I. B. Vendik, O. G. Vendik, M. A. Odit, D. V. Kholodnyak, S. P. Zubko, M. F. Sitnikova, P. A. Turalchuk, K. N. Zemlyakov, I. V. Munina, D. S. Kozlov, V. Turgaliev, A. Ustinov, Y. Park, J. Kihm, and C.-W. Lee, "Tunable metamaterials for controlling THz radiation," IEEE Trans. THz Sci. Techn. **2**, 538–549 (2012).
10. V. Yannopapas and A. Moroz, "Negative refractive index metamaterials from inherently non-magnetic materials for deep infrared to terahertz frequency ranges," J. Phys.: Condens. Matt. **17**, 3717 (2005).
11. M. Plihal, A. Shambrook, A. Maradudin, and P. Sheng, "Two-dimensional photonic band structures," Opt. Commun. **80**, 199–204 (1991).
12. Q. Zhao, J. Zhou, F. Zhang, and D. Lippens, "Mie resonance-based dielectric metamaterials," Mater. Today **12**, 60–69 (2009).

#222877 - $15.00 USD Received 11 Sep 2014; revised 7 Nov 2014; accepted 19 Nov 2014; published 1 Dec 2014

13. K. Vynck, D. Felbacq, E. Centeno, A. I. Căbuz, D. Cassagne, and B. Guizal, "All-dielectric rod-type metamaterials at optical frequencies," Phys. Rev. Lett. **102**, 133901 (2009).
14. D. Felbacq, B. Guizal, G. Bouchitte, and C. Bourel, "Resonant homogenization of a dielectric metamaterial," Microw. Opt. Technol. Lett. **51**, 2695–2701 (2009).
15. Q. Zhao, B. Du, L. Kang, H. Zhao, Q. Xie, B. Li, X. Zhang, J. Zhou, L. Li, and Y. Meng, "Tunable negative permeability in an isotropic dielectric composite," Appl. Phys. Lett. **92**, 051106 (2008).
16. Q. Zhao, L. Kang, B. Du, H. Zhao, Q. Xie, X. Huang, B. Li, J. Zhou, and L. Li, "Experimental demonstration of isotropic negative permeability in a three-dimensional dielectric composite," Phys. Rev. Lett. **101**, 027402 (2008).
17. H. Němec, C. Kadlec, F. Kadlec, P. Kužel, R. Yahiaoui, U.-C. Chung, C. Elissalde, M. Maglione, and P. Mounaix, "Resonant magnetic response of TiO_2 microspheres at terahertz frequencies," Appl. Phys. Lett. **100**, 061117–061117 (2012).
18. H. Němec, P. Kužel, F. Kadlec, C. Kadlec, R. Yahiaoui, and P. Mounaix, "Tunable terahertz metamaterials with negative permeability," Phys. Rev. B **79**, 241108 (2009).
19. L. Peng, L. Ran, H. Chen, H. Zhang, J. A. Kong, and T. M. Grzegorczyk, "Experimental observation of left-handed behavior in an array of standard dielectric resonators," Phys. Rev. Lett. **98**, 157403 (2007).
20. A. F. Oskooi, D. Roundy, M. Ibanescu, P. Bermel, J. D. Joannopoulos, and S. G. Johnson, "MEEP: A flexible free-software package for electromagnetic simulations by the FDTD method," Comput. Phys. Commun. **181**, 687–702 (2010).
21. D. R. Smith, S. Schultz, P. Markoš, and C. M. Soukoulis, "Determination of effective permittivity and permeability of metamaterials from reflection and transmission coefficients," Phys. Rev. B **65**, 195104 (2002).
22. C. R. Simovski, "Material parameters of metamaterials (a review)," Optics and Spectroscopy **107**, 766–793 (2009).
23. V. A. Markel and I. Tsukerman, "Current-driven homogenization and effective medium parameters for finite samples," Phys. Rev. B **88**, 125131 (2013).
24. T. Koschny, P. Markoš, D. R. Smith, and C. M. Soukoulis, "Resonant and antiresonant frequency dependence of the effective parameters of metamaterials," Phys. Rev. E **68**, 065602 (2003).
25. V. Skoromets, F. Kadlec, C. Kadlec, H. Němec, I. Rychetský, G. Panaitov, V. Müller, D. Fattakhova-Rohlfing, P. Moch, and P. Kužel, "Tuning of dielectric properties of $SrTiO_3$ in the terahertz range," Phys. Rev. B **84**, 174121 (2011).
26. X. Chen, T. M. Grzegorczyk, B.-I. Wu, J. Pacheco, and J. A. Kong, "Robust method to retrieve the constitutive effective parameters of metamaterials," Phys. Rev. E **70**, 016608 (2004).

1. Introduction

In the last decades, the quest for a control of interactions between the electromagnetic radiation and matter has given rise to various concepts of arranging matter in different periodic patterns. Specifically, the interest in the optics of photonic crystals (PhCs) was launched mainly by the pioneering works of Yablonovich [1, 2] whose original goals were to achieve a control of light (i) by changes in the light density of states in a periodic structure (inhibition of spontaneous emission, enhancement of the stimulated emission) [1] and (ii) by designing photonic defect states in the band gap able to feature high-Q cavities with a strong field localization and enhancement [1].

About a decade later, a general interest in sub-wavelength periodic structures (metamaterials) arose owing to the Pendry's theoretical work [3–5] aiming to design and describe structures with negative refraction. The word "metamaterial" (MM) appeared first in the paper by Smith *et al.* in 2000 [6] where a structured material with a negative refractive index in the microwave frequency range was experimentally demonstrated. Since then, the concept of MMs has been understood in a broader context as sub-wavelength structures exhibiting artificial (geometrical) electric or magnetic resonances [7]. This development is further gaining strength by the current trends exploiting the advances in miniaturization and nanotechnology.

In both mentioned classes of structures, their properties are due to a resonant behavior at particular frequencies of the electromagnetic field.

1. In MMs, the energy of the resonant field is localized in a small fraction of the unit cell volume, which is usually in/near a resonator made of metal or high-permittivity dielectric ($\varepsilon_r \gg 10$) [8, 9]. The coupling of the resonant field between neighboring cells is

#222877 - $15.00 USD Received 11 Sep 2014; revised 7 Nov 2014; accepted 19 Nov 2014; published 1 Dec 2014

negligible, so the MMs have a small enough spatial dispersion and their behavior can be described using frequency-dependent effective parameters: the index of refraction N_{eff}, wave impedance Z_{eff}, permittivity $\varepsilon_{\mathrm{eff}} = N_{\mathrm{eff}}/Z_{\mathrm{eff}}$ and permeability $\mu_{\mathrm{eff}} = N_{\mathrm{eff}} \cdot Z_{\mathrm{eff}}$.

2. By contrast, PhCs are typically made of low-permittivity dielectrics ($\varepsilon_r \lesssim 12$) which often fill a larger part of volume than what is usual in MMs. The resonances are strongly influenced by the presence of neighboring unit cells as they rely on constructive and destructive interferences between scattered (partially reflected) waves. As a result, the iso-frequency contours of two-dimensional (or three-dimensional) PhCs can deviate from elliptical (or ellipsoidal) shapes which can be described by the standard optics of anisotropic media. In any case, for propagation directions parallel with or close to axes or planes of the structure symmetry, the iso-frequency contours can be locally approximated by surfaces with spherical shapes. Consequently, it is appropriate to introduce an effective index of refraction of the PhC for these particular directions [10].

It appears, however, that some kinds of photonic structures represent intermediate cases between PhCs and MMs; this fact did not receive much attention so far. One of the simplest examples is a square array of cylindrical dielectric rods, oriented parallel to the electric field of the incident wave; this geometry was treated as a photonic crystal [11] and later as a metamaterial [12–14]. The effective response of the rod array depends on two parameters only—the ratio of the unit-cell size a to the rod radius ρ (i.e., the filling fraction $\pi\rho^2/a^2$), and the dielectric permittivity of the rods ε_r. Our aim is to find out which interesting qualitative changes in behavior can be found when these parameters are continuously changed.

In this paper, we discuss numerical results obtained during a systematic variation of the structure parameters. Namely, we show that their relatively minor variations can lead to a qualitatively changing optical response. From the practical point of view, the requirement of a high permittivity $\varepsilon_r \gg 10$ not only restricts the choice of materials but also determines the frequency range where such values can be attained. As a rule, the permittivity in dielectrics decreases in average with frequency except for narrow intervals around resonances, which are always accompanied by an increased absorption. We focus therefore on the microwave and terahertz ranges where materials with a high ε_r exist and the structures can be relatively easily fabricated [15–18]. We assume negligible values of the imaginary part of permittivity and we restrict our computations to the normal incidence, which implies the propagation along the mirror plane inside the photonic structure. In this case, the notion of the refractive index can be used even when the structure is in the PhC regime. In the light of our conclusions, we also re-discuss some earlier published results [13, 19] and summarize the implications for building optical MMs from dielectric rods.

2. Calculation of effective parameters

Our structure [see Fig. 1(a)] is defined by a square unit cell with the linear dimension a periodically distributed in the yz plane; the dielectric rods parallel to x-axis with radius ρ and permittivity ε_r are positioned in the center. The incident wave is polarized $E \parallel x$, periodic boundary conditions were applied in the y-direction. We employed the finite-difference time-domain (FDTD) simulation package MEEP [20] to obtain the scattering coefficients (complex reflectance r and transmittance t) of a structure with variable number of unit cells along the wave vector direction $k \parallel z$. The effective parameters were then retrieved from complex transmittance and reflectance spectra [21]. Alternative means of obtaining the effective parameters are discussed in Ref. [22].

We performed the majority of simulations for a single layer, as its effective properties are almost identical to those of the corresponding multilayer structure. We checked indeed that for this geometry, the retrieved effective parameters depend only negligibly on the number of

#222877 - $15.00 USD Received 11 Sep 2014; revised 7 Nov 2014; accepted 19 Nov 2014; published 1 Dec 2014

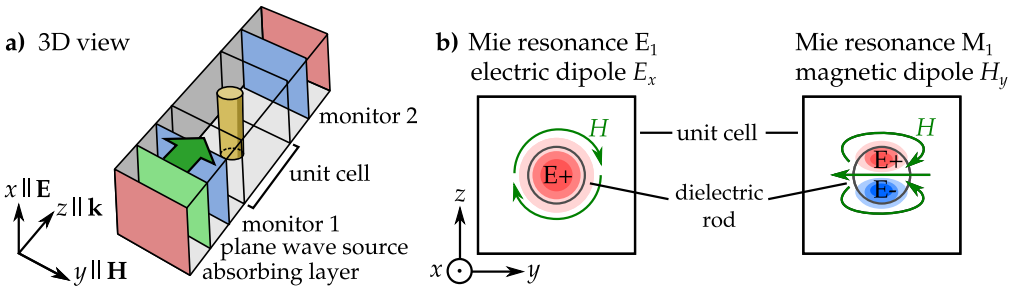

Fig. 1. (a) Perspective view of the unit cell; (b) its cross-sections with the resonant modes excited by a plane wave with $\mathbf{E}||x, \mathbf{H}||y$ and $\mathbf{k}||z$. The first Mie resonance has an electric dipole moment only, while the second one has a magnetic dipole moment instead. The red and blue color shows positive and negative values of the E_x component of the electric field, while the magnetic field is represented by the arrows.

unit cells in the z-direction. The relevance of the calculations with a single layer was further confirmed by current-driven homogenization simulations [23] in several particular cases (same geometries as in Fig. 2) which yielded a response in a very good agreement with the FDTD results.

When inverting the Fresnel-Airy formulas for r and t of our single-layer slab, the correct branches of solutions have to be chosen in the $N_{\text{eff}}(\omega)$, $Z_{\text{eff}}(\omega)$ spectra [22]; to this aim, Kramers-Kronig relations as well as the conditions of a passive medium $\text{Im}(N_{\text{eff}}) > 0$ and $\text{Re}(Z_{\text{eff}}) > 0$ were used, as described in the Appendix. The retrieved value of the complex effective index of refraction $N_{\text{eff}}(f)$ defines the magnitude of the wave vector

$$k(f) = 2\pi f N_{\text{eff}}(f)/c\,. \tag{1}$$

Note that the retrieval procedure described in the Appendix implies that the wave vector introduced by Eq. (1) is defined in an unfolded reciprocal space.

A Bragg resonance occurs when an integer number of half-wavelengths fit into one unit cell, i.e., when

$$k(f) = \frac{q\pi}{a}\,, \tag{2}$$

where q is a non-zero integer. In such a situation, the wave vector is located at a Brillouin zone boundary. The purely real values of k then describe photonic band edges. In a band edge state, a standing wave appears in the structure and it is characterized by exactly q nodal planes dividing each unit cell in the transverse direction to $q+1$ disconnected parts. The band edges delimit a photonic *Bragg band gap* where only evanescent waves described by $N''_{\text{eff}} > 0$ can exist. We can write an equation analogous to (2) for the real part of the refractive index:

$$N'_{\text{eff}}(f) = \frac{qc}{2af}\,; \tag{3}$$

its hyperbolic behavior versus frequency reflects the pinning of the wave vector to the Brillouin zone boundary inside the Bragg band gap.

Another case of interest where evanescent waves are obtained is that of $N'_{\text{eff}} = 0$ (center of the first Brillouin zone, $q = 0$) and $N''_{\text{eff}} > 0$. Here the waves exponentially decay in the medium without any phase change. However, this behavior has a different origin: it is connected to a plasma-like response of the material ($\varepsilon < 0$ or $\mu < 0$) and in this paper we use the term *plasma band gap* to refer to it.

#222877 - $15.00 USD Received 11 Sep 2014; revised 7 Nov 2014; accepted 19 Nov 2014; published 1 Dec 2014

The Kramers-Kronig relations require that for any structure studied, $N'_{\mathrm{eff}}(f)$ [or, equivalently, $k(f)$] attains and finally crosses the Brillouin-zone boundaries when the frequency is sufficiently increased. While usually the convention is used that the corresponding curves are folded back into the first Brillouin zone, in this paper we plot $N'_{\mathrm{eff}}(f)$ in the original (unfolded) Brillouin zones resulting from the retrieval algorithm. This can be clearly observed on the dispersion of the refractive index in Fig. 2. In this way we retain the information about the number of the nodal planes intersecting the unit cell, which is important for our discussion.

3. Results

In the following, we first describe in detail three characteristic cases: we compare the effective parameters computed for three slightly different unit-cell sizes while the rod radius and the dielectric permittivity are fixed. The comparison of these cases reveals quite remarkable changes in the optical behavior of the structure. We then complement this comparison by a continuous scan of the unit-cell sizes in order to obtain an overview of all possible types of the response for the rod-based geometry.

In Fig. 2, we show the calculated reflectance and transmittance amplitude spectra, as well as the effective parameters of three representative structures which have the same rod radii $\rho = 10$ μm, but they differ by the unit-cell size $a = 120$, 100 and 80 μm. These values of a were selected to illustrate three qualitatively different regimes of behavior. The dielectric was defined by a simple lossy model with one high-frequency oscillator, its permittivity was $\varepsilon_r = 100.1 + 0.5\mathrm{i}$ at 500 GHz.

Sparse array In Fig. 2(a), where the unit-cell size $a = 120$ μm, we can see two well separated Mie resonances: the electric one at 680 GHz and the magnetic one at 1030 GHz. The field distribution of the corresponding modes is sketched in Fig. 1(b). The resonance frequencies can be easily identified by an abrupt drop in the real part of the effective index of refraction N'_{eff}, accompanied by a sharp peak in its imaginary part N''_{eff}. The Mie resonances in periodic media must always be adjacent to a Bragg band gap. For instance, in Fig. 2(a) at frequencies below the first Bragg gap, the electric dipoles within each rod are directed along the electric field in the rest of the unit cell. The rods thus positively contribute to the refractive index N'_{eff} which progressively grows until it reaches the first Brillouin zone boundary. At this point, the Bragg condition for a photonic band-gap is fulfilled and each unit cell is intersected by one nodal plane. This is reflected by the dispersion of $N'_{\mathrm{eff}}(f)$ which follows the first Brillouin-zone boundary in the first Bragg band gap between 400 and 680 GHz [equivalent to $q = 1$ in Eq. (3)]:

$$N'_{\mathrm{eff}}(f) = \frac{c}{2af}\,.$$

At 680 GHz, the electric Mie resonance occurs which dramatically changes the near-field photonic properties of the structure. The observed drop in $N'_{\mathrm{eff}}(f)$ and the slope change in $N''_{\mathrm{eff}}(f)$ mark the plasma-like character of the adjacent part of the band gap which extends up to the plasma frequency of the Mie resonance (940 GHz). In this frequency range the electric dipoles in the rods change their direction and induce an electric field opposite to the incident one.

For this sparse array of dielectric rods, the first magnetic Mie resonance lies at 1030 GHz, above the plasma frequency of the electric mode. The second Bragg band-gap opens at 1010 GHz and, due to the Mie resonance, it is transformed to a plasma band gap at 1030 GHz. The next allowed photonic band starts above magnetic plasma frequencies at 1070 GHz. Therefore we observe a very analogous behavior near the magnetic resonance.

For completeness we note that at 1350 GHz, a third Bragg band gap starts which, unlike the lower-frequency ones, does not contain any Mie resonances [see Fig. 2(a)].

#222877 - $15.00 USD Received 11 Sep 2014; revised 7 Nov 2014; accepted 19 Nov 2014; published 1 Dec 2014

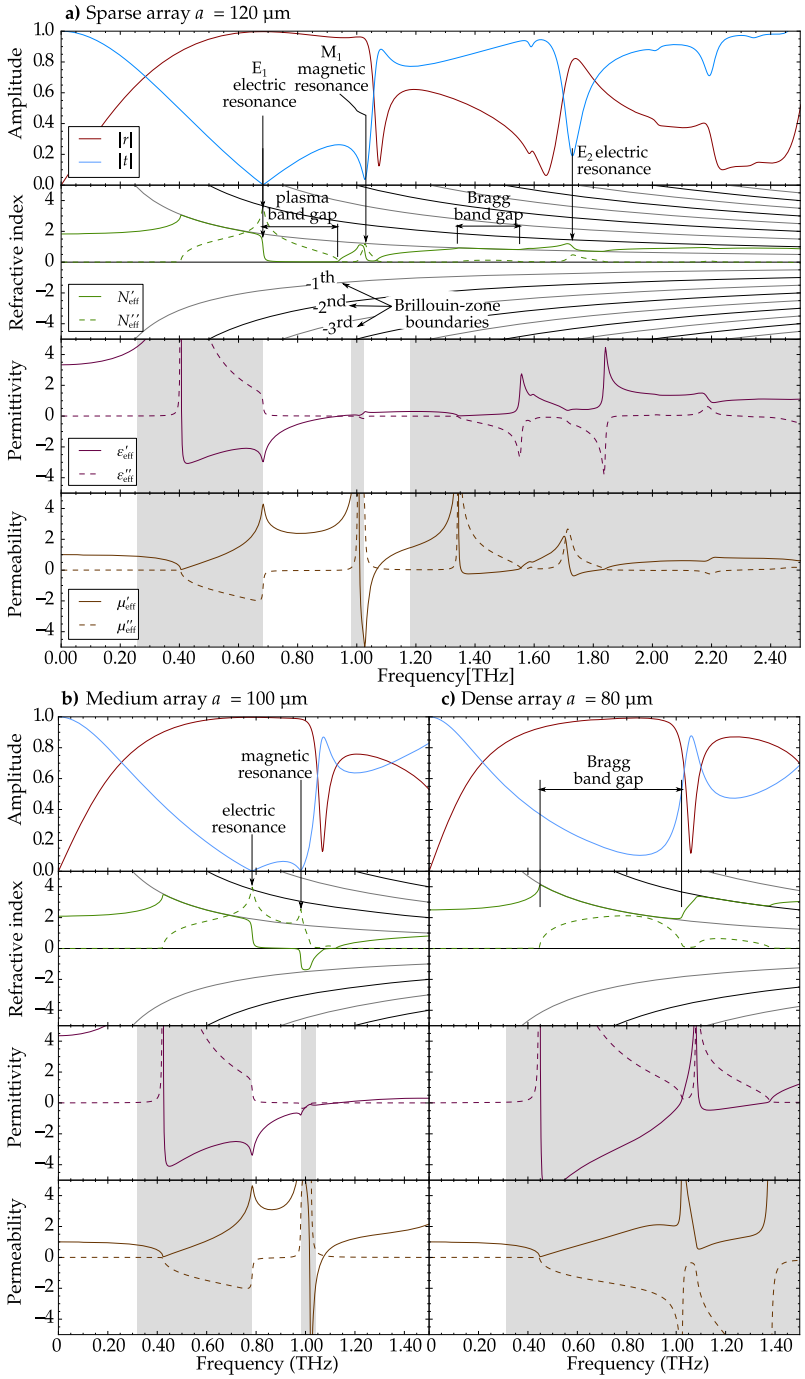

Fig. 2. Results of the FDTD simulations for a single layer of dielectric rods with $\varepsilon_r = 100$, $\rho = 10\,\mu$m. The spectra of reflection $|r|$ and transmission $|t|$ amplitudes share their frequency axes with the retrieved complex effective index of refraction N_{eff}, permittivity ε_{eff} and permeability μ_{eff}, whose imaginary parts are denoted by dashed lines. The frequency ranges where ε_{eff} and μ_{eff} have no physical interpretation (Bragg band gaps or higher order photonic bands) are gray shaded.

#222877 - $15.00 USD Received 11 Sep 2014; revised 7 Nov 2014; accepted 19 Nov 2014; published 1 Dec 2014

The resonances in the effective permittivity $\varepsilon_{\text{eff}} = N_{\text{eff}}/Z_{\text{eff}}$ and permeability $\mu_{\text{eff}} = N_{\text{eff}} \cdot Z_{\text{eff}}$ of a periodic array obviously exhibit shapes very different from the well-known resonance curves of a damped oscillator [24]. In the two separate plasma band gaps we obtain either $\varepsilon_{\text{eff}} < 0$ or $\mu_{\text{eff}} < 0$, i.e. the usual behavior observed in the reststrahlen bands of resonances. However, in the Bragg band gaps occurring just below these spectral ranges the behavior of ε_{eff} and μ_{eff} does not have any useful physical interpretation and it can be understood as a purely formal frequency dependence: we shaded these ranges with light gray in Fig. 2.

Medium array When the unit-cell size is reduced to $a = 100$ μm, as depicted in Fig. 2(b), the Mie resonances shift slightly. Interestingly, in comparison with the sparse array, the electric resonance frequency increases from 680 to 780 GHz, and that of the magnetic resonance decreases from 1030 to 980 GHz. This can be explained by the inter-cell coupling: the circulating magnetic field of the first resonance is compressed when the rods get closer, whereas the magnetic dipoles of the second resonance can couple more easily to each other in the same situation (see Fig. 1).

The converging of the resonance frequencies is linked to the most important qualitative change in the spectra: the fact that the magnetic resonance occurs at a frequency where $\varepsilon'_{\text{eff}} < 0$. The first band gap (the lowest continuous frequency region where $N''_{\text{eff}} > 0$) is thus composed of three adjacent regimes: the first Bragg band gap (425–780 GHz), a plasma band gap (780–980 GHz) and the second Bragg band gap (980–1020 GHz). Every Mie resonance introduces a drop in N'_{eff}, so the following photonic band (1020–1070 GHz) features a negative index of refraction ($N'_{\text{eff}} < 0; N''_{\text{eff}} \approx 0$), i.e., the phase and group velocities are opposite to each other. We conjecture that the presence of two Mie resonances in the *first* combined band gap is a necessary and sufficient condition for $N'_{\text{eff}} < 0$ to occur.

Note that the transmittance amplitude reaches quite small values between the Mie resonances when they are sufficiently close to each other [Fig. 2(b)]. This range forms a well-defined band with a reflectance-to-transmittance contrast much better than that observed in a planar Fabry-Perot resonator. One layer of dielectric rods with proper parameters can therefore be applied as a thin, yet very effective filter.

Dense array Perhaps an even more surprising change occurs when the rod spacing is further reduced. The Mie resonances get even closer in the spectrum and eventually they vanish for $a = 80$ μm [see Fig. 2(c)]. The band gap remains at nearly the same spectral position as in panel (b) of this figure, but, unlike for the medium array, the value of N'_{eff} does not drop within the Bragg band gap. In contrast, it is shifted up to the second Brillouin zone boundary where it meets the second Bragg band gap as clearly seen in panel (c), indicating that each unit cell is intersected by two nodal planes in this state.

The reason of this behavior is related to the change of the nodal plane topology caused by the inter-cell coupling. When the rods are far from each other ($a \gtrsim 100$ μm), the individual Mie resonances create closed regions delimited by a nodal surface where the fields are opposite to the rest of the unit cell. Upon reducing the unit-cell size ($a \lesssim 80$ μm), the regions of opposite fields start to overlap with those from the neighboring cells and the corresponding nodal surfaces interconnect and open. This pair of open nodal surfaces dividing the unit cell manifests itself by a qualitative change of the N'_{eff} spectrum towards a shape typical for one-dimensional photonic crystals.

Continuous scan of the unit-cell size The behavior described above is confirmed by the plots of the complex index of refraction N'_{eff}, N''_{eff} for a continuously varying unit-cell size a from 20 to 200 μm (Fig. 3). Here, again, the constant values of the dielectric permittivity $\varepsilon_r = 100$ and

#222877 - $15.00 USD Received 11 Sep 2014; revised 7 Nov 2014; accepted 19 Nov 2014; published 1 Dec 2014

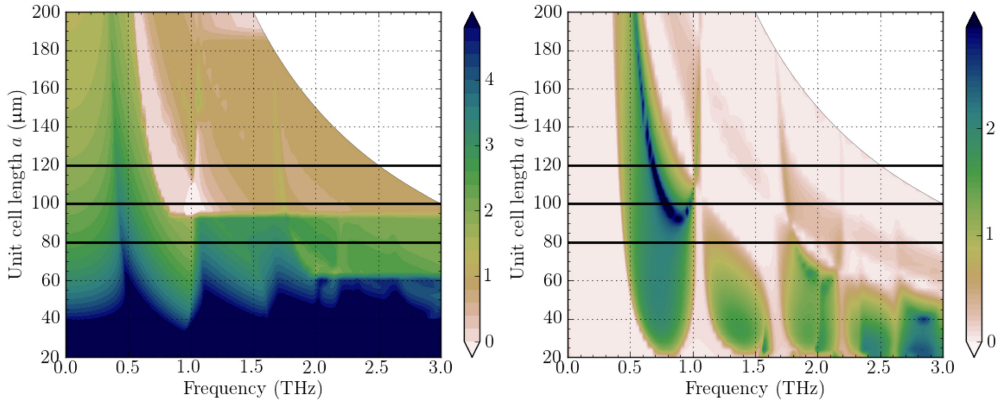

Fig. 3. Real (N'_{eff}, left panel) and imaginary (N''_{eff}, right panel) parts of the refractive index for a dielectric rod array with permittivity $\varepsilon_r = 100$, radius $\rho = 10$ μm and a variable unit-cell size 20 μm $< a <$ 200 μm. The three solid horizontal lines correspond to the values used in Fig. 2.

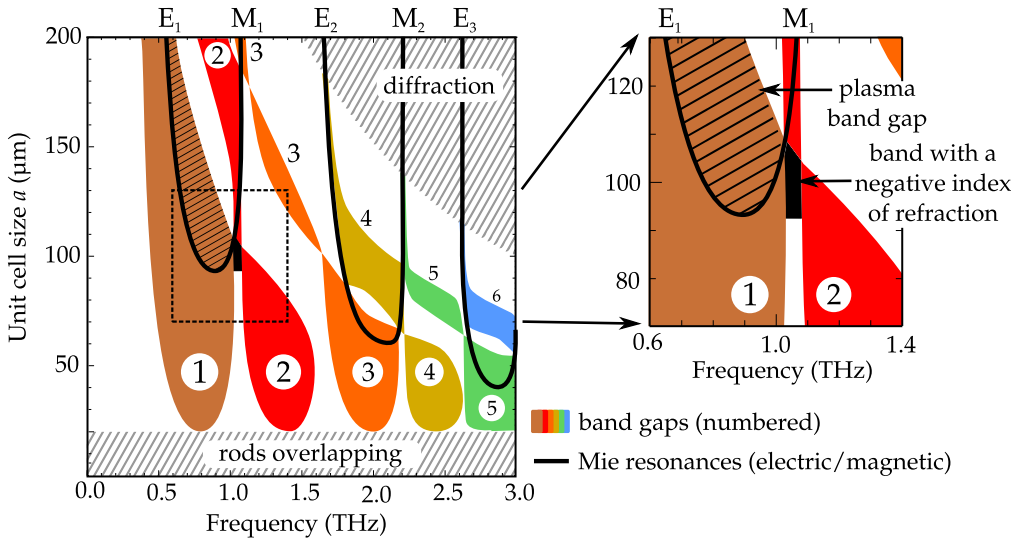

Fig. 4. Scheme of band gaps and Mie resonances under the same conditions as in Fig. 3.

the rod radius $\rho = 10$ μm are used. In the upper-right corner of both plots, for $a > c/f$, an empty area is left where the diffraction prevents the determination of effective parameters.

For an easier interpretation of the results, we draw the most prominent features schematically in Fig. 4. Some of them are common in ordinary one-dimensional photonic crystals, namely, the photonic (Bragg) band gaps which are painted in color in Fig. 4.

The Mie resonances are caused by the field confinement near the high-permittivity rods. They always manifest themselves as sharp peaks in the imaginary part of the index of refraction (N''_{eff}), and in Fig. 4 they are denoted by thick solid curves. Their electric- or magnetic-dipole character is identified by the letters “E” or “M” above the plot, respectively.

As it can be seen in Figs. 3 and 4, the pairs of electric and magnetic Mie resonances form U-shaped curves, at the bottom of which the resonances come closer in frequency to each other and

#222877 - $15.00 USD Received 11 Sep 2014; revised 7 Nov 2014; accepted 19 Nov 2014; published 1 Dec 2014

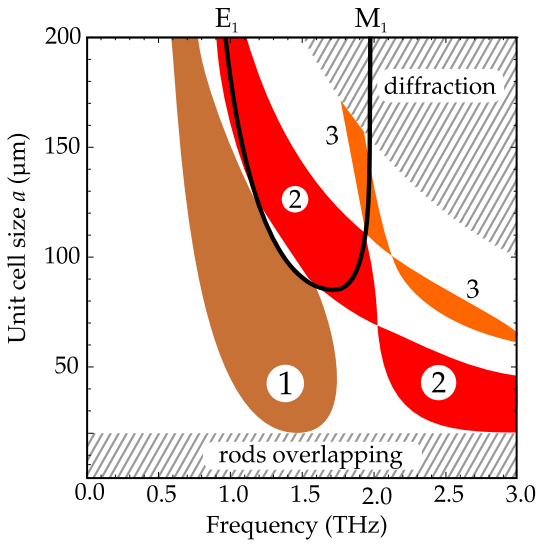

Fig. 5. Scheme of band gaps and Mie resonances for dielectric permittivity $\varepsilon_r = 30$. The Mie resonances shift to higher frequencies relative to the band gaps and no $N'_{\text{eff}} < 0$ region is formed for any unit-cell size (cf. Fig. 4)

eventually they disappear when the unit-cell size a is further reduced. The resonances influence the whole spectra of the refractive index N'_{eff}, so the position of this U-curve delimits the range of a for which a photonic band with $N'_{\text{eff}} < 0$ and $N''_{\text{eff}} \approx 0$ can be found. This negative-index band is shown in black in Fig. 4.

Note that the frequencies of the Mie resonances deviate from their free-space values when the rod distance is reduced. In fact, these resonances help to form the photonic band gaps (both Bragg and plasma band gaps) due to their dispersion. As a consequence, these resonances must be always located inside a frequency range with $N''_{\text{eff}} > 0$.

4. Discussion

Having analyzed the case of high dielectric ($\varepsilon_r = 100$) permittivity rods, we will draw below implications for building a negative-index MM from available dielectrics. Another series of simulations implies that reducing the dielectric permittivity has the main effect to shift all the Mie resonances to higher frequencies (also with respect to the photonic bands). As a result, the band with $N'_{\text{eff}} < 0$ gets gradually narrower and, for the rod permittivity below about 50, we do not find any cell size a that would imply the first and second Mie resonances in the first photonic band as illustrated for $\varepsilon_r = 30$ in Fig. 5. This means that the value of $\varepsilon_r \approx 50$ is the minimum for obtaining a negative index of refraction in any square array of cylindrical rods. Let us note that one would come to a very similar value of minimum permittivity for the case of a square array of bars with a slightly different shape, e.g. a square cross-section.

A sufficiently high permittivity can be found in the microwave and terahertz ranges, in a variety of materials, for example in titanium dioxide with $\varepsilon_r \approx 92$ [18] or in various ferroelectrics like strontium titanate [25]. However, practical applications of the high-permittivity dielectrics in the THz range can be restricted by high dielectric losses due to low-frequency phonon absorption tails. To our knowledge, there is no material providing such a high permittivity in the near-infrared or optical ranges. This eliminates the possibility to build a MM at these frequencies with $N'_{\text{eff}} < 0$ based on dielectric rods.

#222877 - $15.00 USD Received 11 Sep 2014; revised 7 Nov 2014; accepted 19 Nov 2014; published 1 Dec 2014

Finding a valid negative index of refraction N'_{eff} for a photonic structure implies that the Snell law can be used to predict the negative refraction at an interface, provided the iso-frequency contours can be well approximated by a circle. This condition is fulfilled when the resulting wave vector is oriented close to a symmetry axis of the structure, or when the wave vector is negligible compared to the reciprocal-lattice vector (i.e. $k \ll \frac{\pi}{a}$ and thus $|N'_{\text{eff}}| \ll \frac{c}{2af}$). In the latter case the iso-frequency contours of the isotropic structure approach a circular shape near the Γ-point in the Brillouin zone center. By contrast, the opposite implication is not necessarily applicable—a structure with a high enough spatial dispersion can still refract under negative angles, yet its refractive index computed along a symmetry axis never reaches negative values and the phase difference across each its unit cell is positive and can be comparable to π. For example, it was suggested earlier [13] that an array of silicon rods ($\varepsilon_r \approx 12$) can constitute a true left-handed metamaterial ($N'_{\text{eff}} < 0$). In agreement with the results presented above, we believe that the negative refraction is not a sufficient proof of $N'_{\text{eff}} < 0$, which would require a much higher permittivity contrast than that of silicon. We conclude that the electromagnetic behavior observed previously [13] has to be described by means of the PhC dispersion curves.

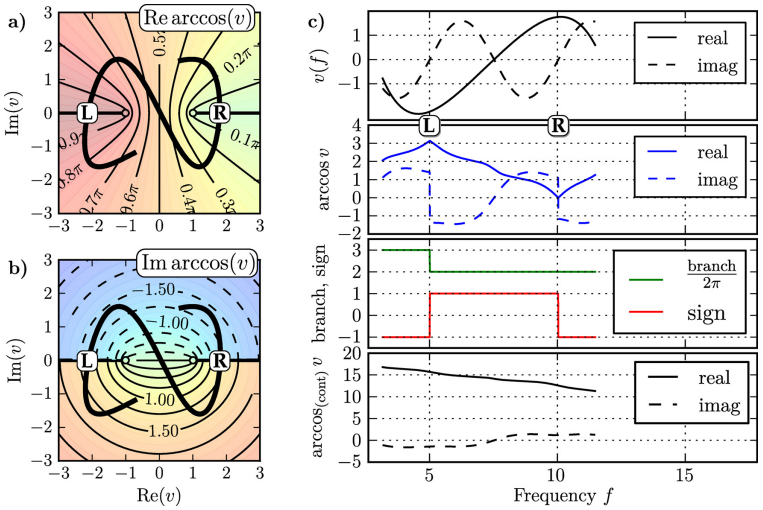

Fig. 6. (a) Real and (b) imaginary parts of arccosine of a complex argument υ; the thick curve shows a possible trajectory of υ (upon a frequency variation), which intersects the branch cuts in points marked as R, L. (c) From top to bottom: example function $\upsilon(f)$, its ordinary arccosine, example branch and sign choices ensuring the continuity of the arccosine function, and $\arccos_{(\text{cont})}\,\upsilon$, as determined by the algorithm described in the Appendix.

We demonstrated that for $N'_{\text{eff}} < 0$, not only the high permittivity contrast, but also a correct geometry is required. A wedge filled with an array of square-shaped high-permittivity bars was previously reported refracting under negative angles [19]. The high filling fraction (0.44^2) simultaneously with a permittivity of $\varepsilon_r \approx 600$ clearly qualified this structure as *dense*. Using the above described approach, we computed its spectra qualitatively similar to Fig. 2(c) and no band with $N'_{\text{eff}} < 0$ was resulting from our effective-index retrieval. However, when we reproduced the wedge experiment numerically, our simulations confirmed that it does refract the light under negative angles.

This structure lies at the boundary between the criteria for MMs and PhCs described in the Introduction. To determine its refraction angle, in general, it is not possible to use the concept of the effective refractive index and its iso-frequency contours have to be used instead (like

#222877 - $15.00 USD Received 11 Sep 2014; revised 7 Nov 2014; accepted 19 Nov 2014; published 1 Dec 2014

in PhCs). At the same time, this structure was proved to partially retain negative refraction even under randomization of the positions of the dielectric bars [19], implying that most of the resonant energy is concentrated inside the dielectric (which is characteristic of MMs).

5. Conclusion

We created and implemented a computational algorithm for a retrieval of effective parameters based on FDTD simulations. Its main asset consists in an automatized and unambiguous determination of the refractive index and impedance spectra $N_{\text{eff}}(\omega)$, $Z_{\text{eff}}(\omega)$. Using this approach, we confirmed numerically that the square array of dielectric rods with a high permittivity ε_r exhibits Mie resonances that can lead to a negative refractive index $N'_{\text{eff}} < 0$.

Based on a parametric scan over the rod density, we demonstrated that there are quite strict requirements for the geometry to obtain a true $N'_{\text{eff}} < 0$. For rods which are too sparse, the electric and magnetic Mie resonances are separated in the spectra [Fig. 2(a)], while for the same rods being too dense [Fig. 2(c)], the Mie resonances come close to each other and disappear; in such a case an ordinary Bragg photonic band gap is formed which does not provide a negative index of refraction.

Apart from the geometric requirements, we found that the existence of the photonic band with $N'_{\text{eff}} < 0$ requires a permittivity of $\varepsilon_r \gtrsim 50$, which limits the selection of materials and the operation-frequency range. It is well known that a similar photonic crystal at optical frequencies can be formed e.g. from silicon ($\varepsilon_r \approx 12$), however its bands of negative refraction will have a high spatial dispersion and the notion of N_{eff} cannot be applied for them.

Appendix: Numerical method

We performed finite-difference time-domain simulations [20] to obtain the frequency (f)-dependent complex reflection $r(f)$ and transmission coefficients $t(f)$ of a sample composed of periodically distributed dielectric rods.

Knowing the complex $r(f)$ and $t(f)$ along with the sample thickness d, we may use the classical algorithm to retrieve the effective parameters [21]:

$$N_{\text{eff}} = \frac{\pm \arccos\left(\frac{1-r^2+t^2}{2t}\right) + 2\pi \cdot m}{k \cdot d} \tag{4}$$

$$Z_{\text{eff}} = \pm\sqrt{\frac{(1+r)^2 - t^2}{(1-r)^2 - t^2}} \tag{5}$$

where $k = 2\pi f/c$ is the wave vector in vacuum and c is the speed of light.

The well-known complication of this approach is that the arccosine and square root are ambiguous functions [22], yielding multiple solutions with different branches (indexed by an integer m) and signs. We deal with a passive medium, consequently we impose $\text{Im}(N_{\text{eff}}) > 0$ and $\text{Re}(Z_{\text{eff}}) > 0$. To facilitate processing of the results, we adopted an approach extending those of earlier published works [21, 26]; our method ensures the continuity of effective parameters as a function of frequency on a purely mathematical basis. This continuity is required by the Kramers-Kronig relations for arbitrarily small losses introduced in the system. The important point consists in identifying the branch cuts of arccosine in the complex plane (Fig. 6(a), (b)). If, by increasing the frequency, the arccos argument, $\upsilon = (1 - r^2 + t^2)/(2t)$, passes through the right branch cut (i.e. for $\upsilon = u + i0$ where $u > 1$), the real part of $\arccos(\upsilon)$ touches zero, whereas the imaginary part is non-zero and changes its sign. The continuity is restored if, from this frequency on, one reverses the sign of the arccos term (point R in Fig. 6(c)). The situation is slightly more complicated at the left branch cut (i.e. for $v = u + i0$ with $u < -1$), where the

#222877 - $15.00 USD Received 11 Sep 2014; revised 7 Nov 2014; accepted 19 Nov 2014; published 1 Dec 2014

imaginary part of $\arccos(\upsilon)$ experiences again a step-like change of the sign and the real part reaches the value of π. The continuity is then restored upon a sign reversal accompanied by a branch index change, illustrated by the point L in Fig. 6(c). A correct reconstruction of the arccosine therefore only requires to compute the integer-valued branch *m* along with the sign, both being functions of frequency. The sign of the square root function is again chosen such that *Z* is a continuous function of frequency.

It is also known that the phase of the reflectance depends on the surface termination for noncontinuous materials. In the cases where the wavelength of the radiation in the material is much larger than the unit-cell dimensions this ambiguity becomes small. A useful control of the effective sample properties can be made by changing the thickness of the sample (number of unit cells along the wave vector). We have chosen a symmetric geometry where the dielectric rod is positioned in the center of a square unit cell and the total thickness of the sample is an integer multiple of the unit-cell size. In this geometry the retrieved effective parameters of our structure depend only negligibly on the number of unit cells that we put in the *z*-direction.

Acknowledgments

This work was supported by the Czech Science Foundation under Grant No. 14-25639S.

#222877 - $15.00 USD Received 11 Sep 2014; revised 7 Nov 2014; accepted 19 Nov 2014; published 1 Dec 2014